



Myosin VI deafness mutation prevents the initiation of processive runs on actin

Olena Pylypenko, Lin Song, Ai Shima, Zhaohui Yang, Anne Houdusse, H Lee Sweeney

► To cite this version:

Olena Pylypenko, Lin Song, Ai Shima, Zhaohui Yang, Anne Houdusse, et al.. Myosin VI deafness mutation prevents the initiation of processive runs on actin. Proceedings of the National Academy of Sciences of the United States of America, 2015, 112, pp.E1201 - E1209. 10.1073/pnas.1420989112 . hal-03059375

HAL Id: hal-03059375

<https://hal.science/hal-03059375>

Submitted on 14 Dec 2020

HAL is a multi-disciplinary open access archive for the deposit and dissemination of scientific research documents, whether they are published or not. The documents may come from teaching and research institutions in France or abroad, or from public or private research centers.

L'archive ouverte pluridisciplinaire **HAL**, est destinée au dépôt et à la diffusion de documents scientifiques de niveau recherche, publiés ou non, émanant des établissements d'enseignement et de recherche français ou étrangers, des laboratoires publics ou privés.

Myosin VI deafness mutation prevents the initiation of processive runs on actin

Olena Pylypenko^{a,b,1}, Lin Song^{c,1}, Ai Shima^c, Zhaohui Yang^c, Anne M. Houdusse^{a,b,2}, and H. Lee Sweeney^{c,2}

^aStructural Motility, Centre de Recherche, Institut Curie, Paris F-75248, France; ^bCNRS, UMR 144, 75248 Paris Cedex 5, France; and ^cDepartment of Physiology, Perelman School of Medicine, University of Pennsylvania, Philadelphia, PA 19104

Edited by James A. Spudich, Stanford University School of Medicine, Stanford, CA, and approved February 3, 2015 (received for review November 4, 2014)

Mutations in the reverse-direction myosin, myosin VI, are associated with deafness in humans and mice. A myosin VI deafness mutation, D179Y, which is in the transducer of the motor, uncoupled the release of the ATP hydrolysis product, inorganic phosphate (P_i), from dependency on actin binding and destroyed the ability of single dimeric molecules to move processively on actin filaments. We observed that processive movement is rescued if ATP is added to the mutant dimer following binding of both heads to actin in the absence of ATP, demonstrating that the mutation selectively destroys the initiation of processive runs at physiological ATP levels. A drug (omecamtiv) that accelerates the actin-activated activity of cardiac myosin was able to rescue processivity of the D179Y mutant dimers at physiological ATP concentrations by slowing the actin-independent release of P_i. Thus, it may be possible to create myosin VI-specific drugs that rescue the function of deafness-causing mutations.

unconventional myosin | deafness | motility | processive movement | omeclamiv

Mysosin VI is unique among the known myosins of animal cells in that it traffics toward the minus end of actin filaments (1). This unique directionality, coupled with its ability to act as both a processive transporter (2, 3) and load-dependent anchor (4), allow myosin VI to play a number of cellular roles that cannot be compensated for by any other myosin motor (5–15). To accomplish these cellular functions, myosin VI has a number of unique structural and functional adaptations, many of which have been debated in the literature, and some are still the subject of controversy (8). This is not surprising because its design features represent significant departures from other characterized myosin motors.

Mutations in myosin VI can result in deafness in humans (16–20). There are three published human mutations (16–18) that cause deafness and result in amino acid changes in the myosin VI motor domain: C442Y, H246R, and E216V. In the mouse, there is one characterized missense mutation (20) in the motor (D179Y) as well as a null mutation (19), both of which result in deafness. All of these mutations likely lead to disruption of the normal organization and maintenance of the stereocilia, the mechanosensing organelles of hair cells, present in the cochlear apparatus, as has been documented in the case of the mouse mutations (19).

Myosin VI achieves its ability to walk hand-over-hand along a single actin filament (21) by having a motor that has been kinetically tuned to spend the majority of its time strongly bound to actin (22). Thus, the probability that at least one head will be strongly bound to actin at all times is very high. (The ratio of the occupancy of the strongly bound actin states of the actin–myosin ATPase cycle to that of the weak + dissociated + strongly bound states is called the duty ratio.) Although a high duty ratio is sufficient for processive movement, processivity can be further enhanced by a mechanism known as “gating” whereby strain between the heads essentially stalls the lead head on actin until the rear head detaches (23). Our proposed mechanism of gating by myosin VI involves blocking of ATP binding to the lead head of a dimer (24, 25). With both a high duty ratio and gating a single myosin VI can move on the order of a micrometer or more along

an actin filament. However, the myosin VI dimer can also function as a load-dependent anchor (4) on actin filaments (as load increases, the attachment time of the dimer greatly increases). This enables myosin VI to play a number of structural roles in cells, such as in the overall organization of the Golgi (26) and in the last step of secretion (27), as well as in formation and maintenance of the stereocilia of the hair cells (16, 19, 20, 28).

Preliminary characterization of the mouse deafness mutation referred to as “tailchaser,” D179Y, revealed an apparent loss of coordination, or gating, between the two heads (20). In the cell, this mutation disrupts endocytosis and results in loss of stereocilia maintenance (20). The impact on endocytosis suggests that the mutation may disrupt processive movement of myosin VI. However, recent *in vitro* experiments suggest that loss of gating should not destroy processive movement (29), and therefore loss of gating would not necessarily lead to deafness. This prompted us to do a much more extensive functional and structural analysis of the impact of the D179Y mutation.

Although myosin VI is unusual in its directionality, structural and kinetic characterizations of the myosin VI actin-activated ATPase cycle have shown that the motor domain of myosin VI adopts structural states and kinetic transitions similar to those of plus-end myosin motors (Fig. 1A). The D179Y mutation belongs to an important region of the motor, which we have called the transducer (30), that lies near the nucleotide-binding site (Fig. 1B and C). This region has been proposed from structural studies

Significance

A number of molecular motors transport cargoes long distances on their cellular tracks as single, dimeric (two-headed) molecules. This processive movement requires specialized kinetic properties (high duty ratio) to ensure that each head of the dimeric motor spends most of its time tightly bound to its track. Additionally, processive motors exhibit intramolecular communication between the heads, called gating, whose importance is less clear. By examining a mutation in the reverse-direction myosin motor, myosin VI, that causes deafness, we provide evidence that the mutation destroys the initiation of processive runs under physiological ATP concentration. We further demonstrate that this defect may be amenable to correction by small-molecule therapeutics.

Author contributions: Z.Y., A.M.H., and H.L.S. designed research; O.P., L.S., A.S., and Z.Y. performed research; O.P., L.S., A.S., Z.Y., A.M.H., and H.L.S. analyzed data; and A.M.H. and H.L.S. wrote the paper.

The authors declare no conflict of interest.

This article is a PNAS Direct Submission.

Freely available online through the PNAS open access option.

Data deposition: Crystallography, atomic coordinates, and structure factors have been deposited in the Protein Data Bank, www.pdb.org (PDB ID codes 4DBP, 4DBQ, and 4DBR).

¹O.P. and L.S. contributed equally to this work.

²To whom correspondence may be addressed. Email: anne.houdusse@curie.fr or lsweeney@mail.med.upenn.edu.

This article contains supporting information online at www.pnas.org/lookup/suppl/doi:10.1073/pnas.1420989112/-DCSupplemental.

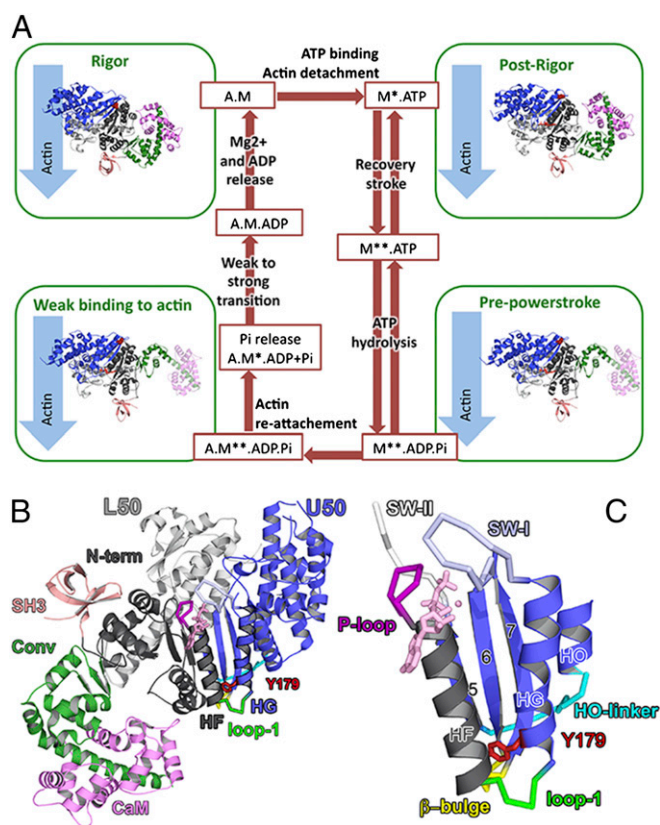


Fig. 1. Actin-myosin chemomechanical transduction cycle and the sub-domain structure of the myosin motor. (A) Actin-myosin cycle. The three structural states crystallized for myosin VI are represented along the motor (ATPase) cycle. (B) Overall structure of the myosin VI D179Y motor domain in the post-rigor state. The position of D179Y is highlighted. The four sub-domains of the motor: N-terminal, U50, L50, and converter are colored gray, blue, white, and green, respectively. The lever arm that amplifies conformational changes of the motor includes the converter and the following elongated region, part of which is represented here as a green helix (insert-2 of myosin VI) to which calmodulin with four Ca^{2+} ions (pink) is bound. (C) Close-up view of the motor domain in a similar orientation as in B. The transducer region lies near the nucleotide-binding site at the junction between the N- and the U50 subdomains. It includes the last three strands of the seven-stranded beta sheet, helices HF and HG, as well as flexible elements such as loop 1, the β -bulge between $\beta 6$ and $\beta 7$, and the HO-linker. Important distortion occurs in the β -sheet as well as rearrangements in the rest of the transducer upon the transitions between states of the actin-myosin cycle.

necessary for the binding of nucleotide and detachment from actin (30, 31). We compared ATP binding and dissociation from actin in the monomeric WT and D179Y mutant myosin VI. As summarized in Table 1 and shown in Fig. 2D, the mutation had little impact on the rate of ATP binding (K_1/k_{+2} in Scheme 1) but greatly slows the ATP-induced detachment of myosin from actin (k_{+2} in Scheme 1, assuming that k_{+8} is extremely fast). This suggests that the mutation slows the transducer rearrangements that are necessary to strongly bind ATP and reopen the actin-binding cleft in response to ATP entering the nucleotide-binding pocket. These rearrangements represent the transition from the rigor state to the post-rigor state (30, 31, 34, 35).

Structures of the Rigor and Post-rigor States. To gain structural insights into the slowing of this rigor to post-rigor transition we crystallized the myosin VI D179Y mutant motor domain + insert 2 (and calmodulin) and determined its structure in the nucleotide-free (rigor) state at 2.2 Å resolution (Table S1). We also

determined the structure in the ATP analog bound state (post-rigor) at 2.6 Å resolution (Table S1). Comparison of the WT and the mutant myosin VI structures revealed that the D179Y mutation causes local structural changes in loop1 and in the following alpha helix (HG) that contains the mutation. In the case of the post-rigor structure, these changes propagate and alter the conformation of the nearby central beta sheet that is part of the transducer (Fig. 4).

It is important to note that there is no impact on the positioning of insert-1 in the rigor state, and in particular no repositioning of L310 (Fig. 5). We have demonstrated that this leucine is in position to provide steric hindrance for the gamma phosphate of ATP and is thus responsible for the relatively slow binding of ATP to myosin VI (K_1/k_{+2} in Scheme 1) and for gating of the myosin VI WT dimer (24, 25).

In the WT rigor state, D179 interacts with two residues of the HF helix, R166 and T169 (Fig. 3). This position of the aspartate corresponds to a conformation of loop1 in which several interactions occur with the β -bulge such as that made by Q176 with the carbonyl of V220. The tyrosine Y179 side chain is bulkier than the aspartate and is directed in the opposite direction. This corresponds to a different arrangement of the main chain of loop1 in this mutant compared with WT (Fig. 3, Figs. S1 and S2, and Movies S1 and S2). Loop1 in the mutant occupies a position that disallows several interactions to be made with the β -bulge while new hydrophobic interactions with the HF and HG helices are made. In particular, the position adopted by residue Q176 drastically differs because it is part of the helix HG in this mutant myosin but not in the WT. The orientation of its side chain toward the solvent cannot allow stabilizing interactions with the transducer as are seen in the WT myosin.

Table 1. Steady-state and transient kinetic parameters of WT and D179Y myosin VI-MD^{ins2}

Kinetic parameters	MVI-MD ^{ins2} WT	MVI-MD ^{ins2} (D179Y)
Steady-state parameters		
$V_{\text{MAX}}, ^\circ \text{s}^{-1}$	6.6 ± 0.3	1.9 ± 0.4
$K_{\text{ATPase}}, ^\circ \mu\text{M}$	12.4 ± 0.2	NA
$V_0 (-\text{actin}), ^\circ \text{s}^{-1}$	0.11 ± 0.1	1.2 ± 0.6
Rate constants of the actomyosin VI ATPase cycle (Scheme 1)		
$k_{+4A}': \text{P}_i \text{ release with actin}, ^\circ \text{s}^{-1}$	121 ± 4.2	133 ± 8.3
$k_{+4A}: \text{P}_i \text{ release } (-\text{actin}), ^\circ \text{s}^{-1}$	0.3 ± 0.1	58.1 ± 10.3
$k_{+4B}': \text{Weak-to-strong transition on actin } (k_{+4B})^5$	28.3 ± 0.58	38.6 ± 3.1
$k_{+5}': \text{ADP release from actomyosin VI}, ^\circ \text{s}^{-1}$	7.0 ± 0.08	2.03 ± 0.07
$k_{+5}: \text{ADP binding to actomyosin VI}, ^\circ \mu\text{M}^{-1} \cdot \text{s}^{-1}$	0.57 ± 0.29	0.51 ± 0.10
$k_{+5}: \text{ADP release } (-\text{actin}), ^\circ \text{s}^{-1}$	8.5 ± 0.18	2.6 ± 0.18
$k_{+5}: \text{ADP binding } (-\text{actin}), ^\circ \mu\text{M}^{-1} \cdot \text{s}^{-1}$	1.2 ± 0.34	0.49 ± 0.17
ATP-induced dissociation from pyrene-actin		
$k_{+2}, ^\circ \text{s}^{-1}$	568 ± 24.9	79.1 ± 5.1
$K_1/k_{+2}, ^\circ \text{mM}^{-1} \cdot \text{s}^{-1}$	13.9 ± 1.2	14.2 ± 3.0

NA, not assessed.

^{*}Measured in the NADH coupled assay.

[†]Steady-state turnover in the absence of actin.

[‡]Measured using phosphate-binding protein (PiBiP).

[§]Measured with pyrene actin.

[¶]Measured with mantADP.

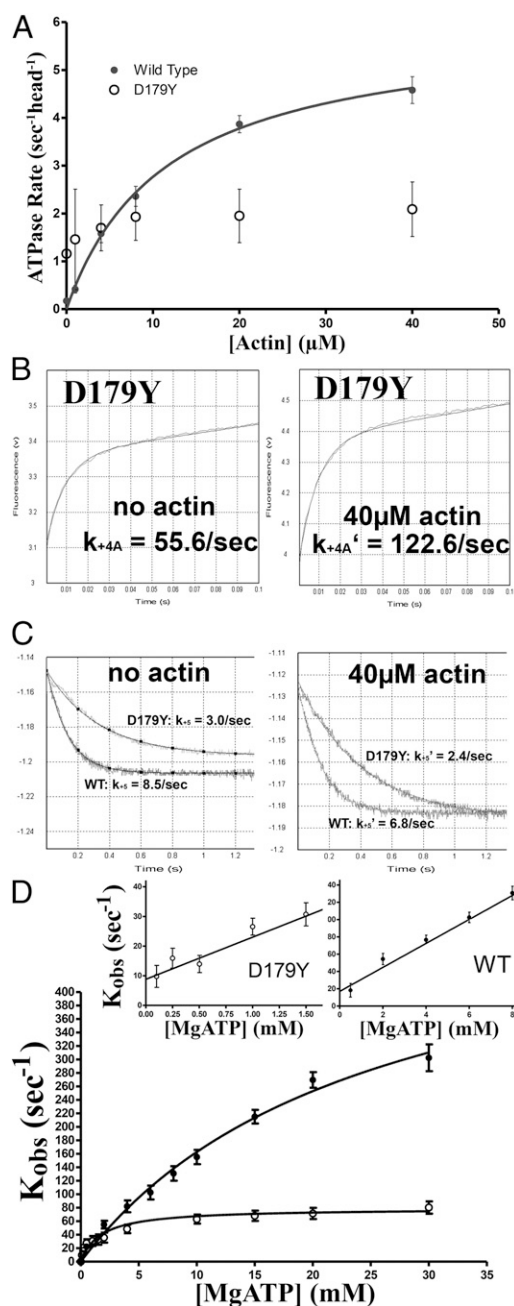


Fig. 2. Major kinetic alterations of the D179Y mutation in myosin VI. (A) The actin concentration dependence of the steady-state ATPase activities (s⁻¹ per head) of single-headed (MVI-MD^{ins2}) myosin WT (●) and VI-D179Y (○) are shown as an average of four preparations. The maximal actin-activated ATPase for WT and the D179Y mutation were $6.6 \pm 0.3/\text{s}$ and $1.9 \pm 0.4/\text{s}$, respectively. Note that in the absence of actin the mutant activity is $1.2 \pm 0.6/\text{s}$. Thus, the D179Y mutant shows less than a twofold activation with actin, whereas the WT has an approximately 60-fold activation. (B) Stopped flow traces representing phosphate release from the D179Y mutant in the presence and absence of actin are shown. The smooth line in each panel is a single exponential fit to the data. The fits gave a phosphate release rate (k_{+4A}) of 55.6/s in the absence of actin and a release rate (k_{+4A}') of 122.6/s in the presence of actin. (C) Shown are stopped flow traces representing ADP release (mantADP dissociation) from WT and D179Y mutant myosin VI in the absence and presence of actin. Single exponential fits (solid lines) gave ADP dissociation rates in the absence of actin (k_{+5}) and in the presence of actin (k_{+5}') that were about threefold slower for the D179Y mutant than for WT. (D) The rate of ATP-induced dissociation of single-headed myosin VI (rigor) from actin (as monitored by the rate of enhanced pyrene-actin fluorescence) is plotted as a function of MgATP concentration. The maximal

The most dramatic structural perturbations of the D179Y mutation are in the postrigor state in which loop1, the alpha helix (HG), and also the central beta sheet conformation, which are part of the transducer, are all affected. Because the transducer undergoes distortion between the rigor and postrigor states upon ATP binding to the motor, the perturbation to the beta sheet seen in the postrigor conformation, together with the difficult rearrangement of the bulky tyrosine 179 side chain during the transitions (see below), likely causes the observed slowing of the transition from rigor to postrigor (i.e., detachment from actin).

In the postrigor state, D179 interacts with the amide groups of T174 of loop1 (Fig. 3). It is found at the surface of the molecule and is not involved in interactions with the transducer beta strands. In contrast, the tyrosine D179Y side chain adopts a position buried in the structure below the HF helix and loop1 and interacts with the β -bulge (residues F214–V220) of the transducer (Fig. 3 and Movies S1 and S2). This results in large differences in the conformation of both the HG helix orientation and the rest of the transducer (Fig. 4). The difference in the conformation of loop1 in the mutant and WT structures also contributes to generate specific interactions between Q176 and the β -bulge in the mutant myosin that do not occur in the WT structure. Whereas in the WT specific interactions between loop1 and the rest of the transducer mediated by Q176 occur only in the rigor state, not in the postrigor or the PPS states, the mutation induces more specific interactions to occur between loop1 and the rest of the transducer in the postrigor state but not in the rigor and PPS states of the mutant myosin VI.

These structural differences explain why the kinetics of the transition between the rigor and postrigor states that allows detachment from actin are much slower in the mutant compared with WT myosin VI. The D179Y mutation will make the structural transitions of the ATPase cycle more difficult owing to the Y179 stabilizing hydrophobic interactions and to steric clashes involving the bulky Y side chain that occur in the course of the transitions between rigor and postrigor that allow detachment of the motor from actin (Fig. 3 and Movies S1 and S2).

Loss of Gating Does Not Destroy Processive Runs. It has been suggested that gating is not necessary for processive movements by myosin and all that is required is a high duty ratio (29). Gating in myosin VI normally is due to an asymmetry in the rates of ATP binding to the two bound heads of a processive dimer, with ATP binding to the lead head occurring at a much slower rate than to the rear head (24). To assess the impact of loss of gating without changing the mechanical properties of the myosin lever arms, as was done in earlier studies (29), we examined the L310G mutation in myosin VI. We previously demonstrated that the side chain of this leucine is positioned to hinder entry of the gamma phosphate into the nucleotide-binding pocket (25). Kinetic characterization of this L310G mutation showed that replacement of L310 with a glycine resulted in an ATP binding rate that was similar to that of other myosins that lack insert-1 and abolished gated ATPase activity of a myosin VI dimer (25). We performed single-molecule motility experiments also with the L310G mutant in the presence of 3 mM ATP, as for WT myosin VI. Compared with WT myosin VI (Fig. 6A), the L310G myosin VI dimer is processive (Fig. 6B), but with shorter run lengths

dissociation rate (k_{+2}') for the D179Y mutation plateaus at $79.1 \pm 5.1/\text{s}$, whereas the extrapolated maximal value for the WT is $568 \pm 25/\text{s}$. The slope of the linear phase at low actin concentrations allows an estimation of the rate of ATP binding ($K_1 k_{+2}'$), which is unchanged by the D179Y mutation (Table 1). The insets are the expanded linear portions of the D179Y and WT ATP-induced dissociation relationships, which gave values of $14.2 \pm 3.0 \text{ mM}^{-1} \text{ s}^{-1}$ and $13.9 \pm 1.2 \text{ mM}^{-1} \text{ s}^{-1}$, respectively, for $K_1 k_{+2}'$.

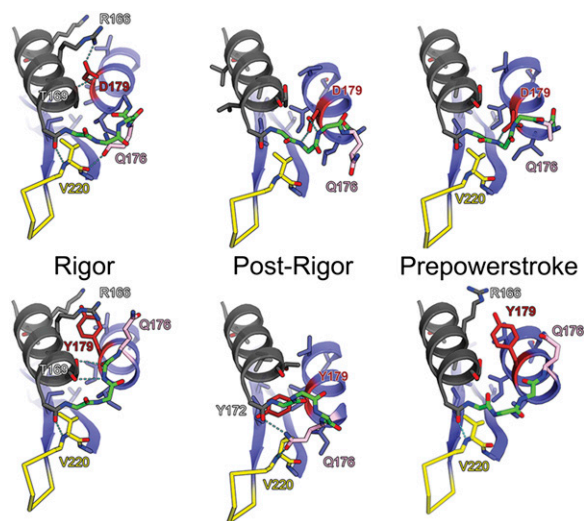


Fig. 3. Close-up view of the structural arrangement near the D179Y mutation. Part of the transducer region, including the HF-loop1–HG module and the beta-5 and beta-6 strands of the central beta sheet are compared for the MVI-WT and MVI-D179Y mutants in rigor, post rigor, and PPS conformational states (HF helix, gray; HG helix, blue; loop1, green; β -bulge, yellow). The residues making stabilizing interactions are shown in sticks, and hydrogen bonds are shown in dashed lines. Note in particular the differences in the interactions between these helices and the rest of the transducer.

than the WT myosin VI dimer (mean run lengths were $1.2 \pm 0.1 \mu\text{m}$ for WT and $0.9 \pm 0.1 \mu\text{m}$ for the L310G mutant.)

Single-Molecule Motility of D179Y. Our kinetic measurements and the reported mouse phenotype (20) suggest that single-molecule processive movements will be impaired by the D179Y mutation. Indeed, under conditions (3mM ATP and no ADP) where we see robust processive single-molecule runs by our WT myosin VI dimer (Fig. 6A) we cannot detect any single-molecule movement by the D179Y dimer. Raising the ADP concentration to 10 or 100 μM while keeping the ATP at 3 mM did not rescue movement by the mutant, even though it increases processive run lengths of the WT molecule (24).

To establish that myosin VI with the D179Y mutation is capable of movement, although it is not processive, we examined the ability of multiple dimeric (HMM) molecules to move actin filaments in bulk motility assays (gliding actin filament assays). As shown in Fig. 6C, the mutant protein does display motility, but at a velocity that is about a third that of the WT. This is consistent with the slower ADP release rate of the mutant (k_{+5}' in Table 1).

Rescue of Processivity with Rigor Binding or Lowering ATP. The kinetics in the presence of actin suggest that the molecule has a higher duty ratio than does WT and therefore processivity might be possible if both heads could bind simultaneously to actin. We postulated that processive movement might be rescued if both heads of a dimer are bound to actin in rigor and then ATP is added to initiate processive movement, owing to the gating mechanism discussed above. That head would then detach more rapidly, initiating processive movement on actin. This prediction was borne out in experiments that revealed processive movement could be seen for the D179Y mutation when 3 mM ATP was added to dimers that were bound in the absence of nucleotide to actin filaments (Fig. 6D). To test whether initiation of the processive movement observed with the D179Y mutant dimer under following rigor binding depends on the gating mechanism of myosin VI (Fig. 7) we introduced the L310G mutation along with

the D179Y mutation into a zippered myosin VI dimer. In this case, no single-molecule movement was observed following rigor binding and addition of 3 mM mgATP. These experiments directly support the mechanism of myosin VI gating and the proposed impact of the D179Y mutation as depicted in the model of Fig. 7 and presented in Discussion.

Using this same approach, the WT dimer processive movement was essentially identical to that observed in Fig. 6A: The mean run length was $1.1 \pm 0.2 \mu\text{m}$, with a run length decay constant of $0.8 \mu\text{m}$. Note that following rigor binding and ATP addition we observed many fewer runs for the D179Y mutant dimer than for WT because we only observed movement immediately after ATP addition. This is because once dimers detach from actin at the end of a run they cannot rebind and initiate processive runs. The run length was less than that of the WT, with a mean run length of $0.6 \pm 0.5 \mu\text{m}$ and run length decay constant of $0.5 \mu\text{m}$. (For WT the respective corresponding values were $1.2 \pm 0.1 \mu\text{m}$ and $0.8 \mu\text{m}$.) The mean velocity was about a third of the WT value for the mutant ($0.2 \pm 0.1 \mu\text{m/s}$ compared with $0.6 \pm 0.2 \mu\text{m/s}$). This would be expected given that the ADP release rate (k_{+5}') is about a third that of WT and indicates that the average step size is not markedly changed.

We also reasoned that lowering the ATP concentration would allow the rear head of a dimer to remain attached for a longer period, allowing the lead D179Y mutant head sufficient time to attach to actin and initiate a processive run. When the ATP concentration was lowered to 0.1 mM processive runs were observed with both WT dimers and dimers of D179Y. The mean

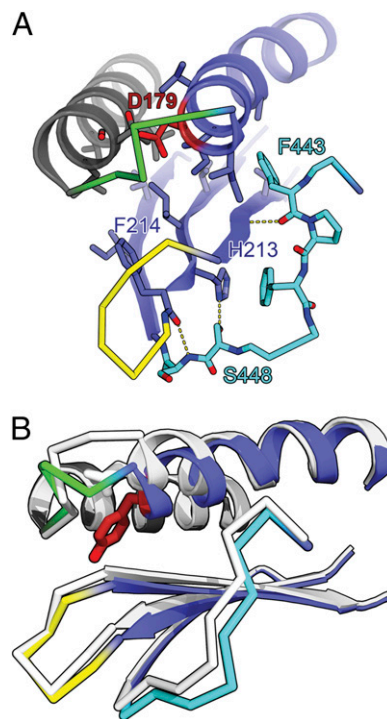


Fig. 4. Differences in the transducer conformation introduced by the mutation in the post rigor state. (A) Conformation of the transducer in the post rigor WT structure. The interactions between elements of the transducer that are conserved in all structural states are indicated. They also occur in the three structural states of the D179Y mutant and lead to a rigid body movement of the beta sheet for the post rigor state of the MVI-D179Y owing to the introduction of the Tyr179 side chain, as shown in B. (B) Superimposition of the MVI-WT (white) and the MVI-D179Y (colored) structures in the post rigor state show how the transducer rearranges to accommodate the burial of the Y179 mutated side chain.

run length for the WT was $0.7 \pm 0.1 \mu\text{m}$ and run length decay constant was $0.5 \pm 0.1 \mu\text{m}$. For the D179Y dimer, the mean run length was $0.6 \pm 0.2 \mu\text{m}$ and run length decay constant was $0.4 \pm 0.2 \mu\text{m}$ (Fig. 6E).

Discussion

Kinetic data (Table 1) reveal multiple effects of the D179Y mutation, and our initial conclusion that the mutation destroys gating (20) was incorrect. The primary defect that destroys processive movement is an uncoupling that allows rapid P_i release in

the absence of actin. This uncoupling leads to loss of processive movement at physiological ATP concentrations. However, processive movement can be rescued if both heads are initially bound in rigor (absence of nucleotide) to an actin filament. Although

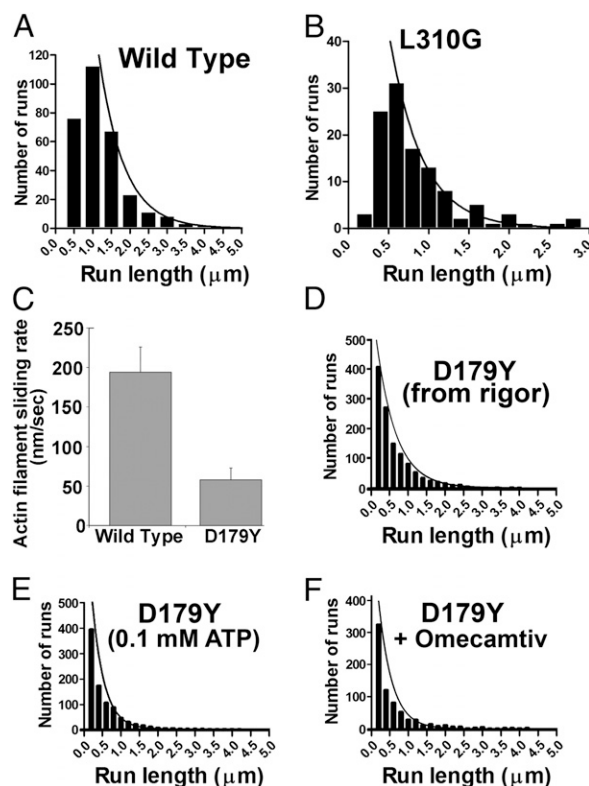


Fig. 6. Motility of WT and mutant myosin VI dimers. (A) Single-molecule motility of the WT myosin VI dimer. Shown is the run length distribution for processive myosin VI dimers. The mean run length was $1.2 \pm 0.1 \mu\text{m}$ and the run length decay constant (as determined from the fit indicated in the figure) was $0.8 \mu\text{m}$. The dimers of the D179Y mutant did not move as single molecules in this assay at 3 mM ATP. (B) Single-molecule motility of the L310G mutant myosin VI dimer. Shown is the run length distribution of the L310G mutant dimer, which displays a shorter average run length than WT (A). The mean run length was $0.9 \pm 0.1 \mu\text{m}$ and the run length decay constant (as determined from the fit indicated in the figure) was $0.7 \mu\text{m}$. (C) Gliding filament assays for WT and D179 mutant myosin VI dimers. Shown is the average actin filament sliding rate for the concerted actions of multiple myosin VI dimers acting upon an actin filament. Note that this assay reveals that the concerted actions of multiple D179Y mutant dimers are capable of moving actin filaments, but with a lower velocity than the WT dimers. (D) Single-molecule motility of the D179Y mutant myosin VI dimer initiated by rigor binding. Shown is the run length distribution of the D179Y mutant dimer, which is only observed if the dimer is first bound to actin in the absence of nucleotide (rigor) and then 3 mM ATP is added to initiate processive runs. The mean run length was $0.6 \pm 0.5 \mu\text{m}$ and run length decay constant was $0.5 \mu\text{m}$ (as determined from the fit indicated in the figure). Under these conditions, the D179Y dimer displays a shorter average run length than WT (A). (E) Single-molecule motility of the D179Y mutant myosin VI dimer at 0.1 mM ATP. Shown is the run length distribution of the D179Y mutant dimer when the MgATP concentration is lowered to 0.1 mM. The mean run length was $0.6 \pm 0.6 \mu\text{m}$ and run length decay constant was $0.4 \mu\text{m}$ (as determined from the fit indicated in the figure). (F) Single-molecule motility of the D179Y mutant myosin VI dimer at 3 mM ATP and $20 \mu\text{M}$ omecamtiv. Shown is the run length distribution of the D179Y mutant dimer at 3 mM ATP in the presence of $20 \mu\text{M}$ omecamtiv (to stabilize the PPS state in the absence of actin). The mean run length was $0.5 \pm 0.6 \mu\text{m}$ and run length decay constant was $0.4 \mu\text{m}$ (as determined from the fit indicated in the figure). Without the addition of omecamtiv, the D179Y dimer does not display single-molecule processive movement at this physiological ATP concentration.

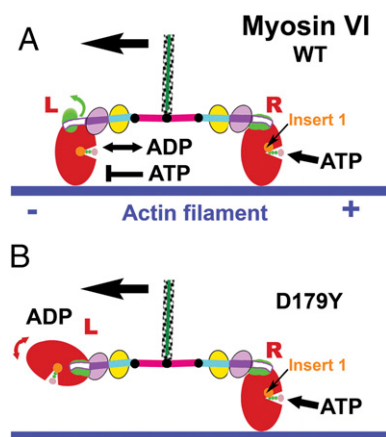


Fig. 7. Schematic models representing the normal gating mechanism of myosin VI and disruption by the D179Y mutation. (A) Model illustrating the gating mechanism of myosin VI in which the lead head of a dimer is stalled in a state that can bind ADP but not ATP. (B) In the case of the D179Y mutant, premature release of phosphate places the unbound head in a conformation that cannot rapidly attach to actin. In this case, ATP will cause detachment of the bound head before the unbound head can bind to actin, thereby terminating or preventing a processive run.

most of the kinetic steps are somewhat affected, the largest effects are a slowing of ADP release when bound to actin (k_{+5}'), with a concomitant slowing of the actin-activated ATPase rate (ADP release is the rate-limiting step), and a slowing of ATP-mediated detachment of actin from myosin (k_{+2}') (but no slowing of ATP binding to myosin: K_1/k_{+2}'). Because the mutation is within and distorts the transducer region of the motor, these kinetic data suggest that major transducer rearrangements must occur during the transition from the strong ADP-binding actin–myosin state to rigor, and during the transition from rigor to postrigor. The latter transducer rearrangement has been documented at high resolution (30, 34, 35) whereas the former has not, because there is no high-resolution structure for the strong ADP-binding actin–myosin state.

The lack of high-resolution structural data for the states populated during the powerstroke is a major remaining challenge necessary to describe how myosin produces force. The kinetic and structural data of this D179Y mutation bring insights for the myosin force production mechanism by implying which conformational changes associated with product release are linked to a transducer rearrangement. Analysis of the myosin VI-D179Y structures present in Figs. 3 and 4, [Figs. S1](#) and [S2](#), and [Movies S1–S3](#) provides an explanation as to why both ADP release and ATP-induced detachment from actin are slowed. The D179Y mutation should make all structural transitions of the ATPase cycle that involve transducer rearrangements more difficult owing to the stabilizing hydrophobic interactions and steric clashes involving the tyrosine Y179 side chain (Fig. 3 and [Movies S1](#) and [S2](#)). ADP release, which is the slowest step of the actomyosin ATPase cycle, is reduced approximately threefold compared with WT myosin VI. Thus, we would predict that a significant transducer rearrangement would occur in the transition that releases ADP and forms the rigor state. This would require a repositioning of the Y179 side chain. This is consistent with FRET studies that have detected a change within the U50 subdomain upon ADP release (37).

Interestingly, the early steps of the powerstroke upon reattachment to actin, the P_i release and the following step, the weak-to-strong transition, are less affected by the D179Y mutation (Table 1) and are slightly increased in rate. [The weak-to-strong transition is defined by the quenching of pyrene-labeled

actin (22) and results in formation of a state that strongly binds both MgADP and actin.] This result suggests that the D179Y mutation favors a transducer conformation that allows MgADP to remain tightly bound following release of P_i and simultaneously allows at least partial closure of the actin-binding cleft to create a strong actin-binding interface. How this is achieved cannot be predicted from existing structures.

Myosin VI with the D179Y mutation has an elevated basal ATPase rate owing to rapid release of P_i , implying that the PPS conformation (which traps P_i) is not as stable compared with WT. The structures of this mutant in different states provide some insights into why this may be the case. Lack of stabilization of loop1 and the fact that the tyrosine side chain is rather solvent-exposed in the PPS state could favor a transition to a state(s) in which the tyrosine would be more buried (as in the postrigor state). Although we do not know the state to which this mutant rapidly transitions from the PPS state in the absence of actin, the state must be unable to trap phosphate in the motor and likely results in a lever arm swing that prevents the head from remaining in the proper geometry required for easily finding actin-binding sites when it is the lead head of a dimer. This highlights how essential it is for processive myosins to stabilize the PPS state and trap phosphate in the absence of actin. For processive stepping, it is critical to keep the lead head in the appropriate geometry to enable rapid actin binding.

The D179Y mutation destroys processivity under conditions in which the myosin is introduced to actin filaments in the presence of physiological [ATP]. This is due to the fact that when the dimer encounters actin and one head binds there is a high probability that the unbound head will have ADP bound rather than ADP· P_i . Our modeling of this conformation, schematized in Fig. 7B, suggests that it does not allow rapid binding to actin. This geometrical constraint on binding of the unbound head of a dimer would allow ATP binding to the bound head (following ADP release) to detach the dimer from actin, before binding of the unbound head to actin, rendering initiation of processive movement impossible.

Under conditions where ATP is introduced after the D179Y dimer is bound to actin, processive runs are observed. If no ATP is present, then both heads will bind to actin. Upon introduction of ATP to the rigor-bound dimers, ATP can bind to the rear head, but the gating mechanism of myosin VI (Fig. 7A) prevents binding of ATP to the lead head until the rear head detaches from actin. This allows initiation of the processive run. Ablation of gating, by introducing the L310G mutation in addition to the D179Y mutation, prevents initiation of processive runs following introduction of ATP to dimers bound in rigor. These experiments suggest that gating could have an unrecognized, but important, role in the initiation of processive runs of WT dimers as well.

The mechanism by which the D179Y mutant destroys processive movement is not a disruption of normal ATP gating, as we have shown for the L310G mutation (25). Disruption of normal gating by the L310G mutation decreases the processive run lengths but does not destroy processive movement (Fig. 6B). Decreased run length is consistent with other mutations in myosin VI that have interfered with head coordination by possibly altering the physical coupling between the heads (29). In these cases, because both heads can readily attach to actin, the degree of processivity is a function of the duty ratio (i.e., the percentage of the overall cycle that the head is strongly bound to actin). The kinetics of the D179Y mutant would tend to increase the duty ratio, thus suggesting that it fails to be processive solely owing to geometric constraints linked to the disruption of product trapping by the detached myosin head that hinder its attachment to actin before ATP-induced release of the rear head.

Interestingly, a human deafness-causing mutation also found in the transducer, C442Y, has been reported to activate the

steady-state ATPase activity in the absence of actin and seems to disrupt processivity (38). However, unlike the D179Y mutation, the C442Y mutation greatly increases the rate of ADP release, which in turn will greatly reduce the duty ratio. Thus, this mutation in the transducer destroys processive movement via two different mechanisms, namely, reducing the duty ratio and uncoupling phosphate release.

The conclusion that the D179Y mutation severely limits initiation of processive movement, which in turn impairs transport by myosin VI, fits well with the observed cell biological manifestations of the mutation in hair cells. These include disorganized hair-cell stereocilia of the cochlear apparatus (resulting in deafness) and impaired endocytosis (20). The mutant myosin VI accumulates at the tips of the stereocilia (20), which would be expected if the motor cannot efficiently initiate movement toward the base (its normal minus-end directed movement on actin). Myosin VI was also found along the stereocilia and at the base to lesser extents (20). The cellular phenotype in the D179Y Tailchaser mice is less severe than in the myosin VI null Snell's waltzer mouse (19), however. This may be due to partial functionality of the D179Y myosin VI because multiple molecules can generate movement on actin.

An interesting implication of the single-molecule and kinetic data is that the myosin VI molecules must be present and working at very low density on both endocytotic vesicles and on their targets within the stereocilia. Our motility data (Fig. 6C), indeed, indicate that a number of closely spaced dimers, or even closely spaced monomers, bearing the D179Y mutation would allow movement. Based on the fact that myosin VI functions optimally as a dimer (39), and that at least a subset of its cargoes induce dimerization, we have proposed that myosin VI likely functions as a dimer in cells (8, 40). It would seem that, because the major impact of the D179Y mutation is to prevent the binding of the lead head of a dimer, myosin VI likely functions as a dimer for the cellular functions involving the maintenance of stereocilia and endocytosis. Consistent with this, we recently published evidence that myosin VI must dimerize to perform its roles in endocytosis and Golgi maintenance in fibroblasts (39).

We were also able to rescue processivity of the D179Y mutant at physiological ATP concentrations by using high levels (20 μ M) of the cardiac myosin activator drug omecamtiv. Although the run lengths were somewhat less than those of WT and the movement was slower, the level of activity may be sufficient to rescue in vivo function. Unfortunately, the D179Y mice no longer exist, so the compound cannot be tested in vivo. Additionally, the dose used to rescue processivity of the myosin VI D179Y was 100-fold higher than the efficacious in vivo dose for enhancing cardiac function (36), and thus could lead to cardiac toxicity as well as off-target effects on other myosin classes. Thus, it is unlikely that omecamtiv can be used to correct the effects of myosin VI mutations, such as the D179Y or C442Y, in mice or humans. Our data suggest, however, that it may be feasible to develop myosin-VI specific drugs that can counter the impact of deafness-causing mutations.

Methods

Protein Constructs and Expression. A series of truncations of porcine myosin VI cDNA with the D179Y mutation were generated. C-terminal truncations were made corresponding to amino acid 816 [D179Y MD^{ins2}, D179Y delta-insert1 MD^{ins2} (in which residues C278 to A303 have been deleted)], to amino acid 789 (D179Y MD), and to amino acid 839 (D179Y S1). Each of these had a Flag tag (encoding DYKDDDDK) appended via a glycine to either the N terminus (MD, MD^{ins2}) or the C terminus (S1) to facilitate purification. As previously described (24), a "zippered" dimer myosin VI construct (HMM) was created by truncation at Arg-994, followed by a leucine zipper (41) to ensure dimerization. This sequence was followed by myc and Flag tags for motility assays and purification, respectively, as described previously (42). These constructs were used to create a baculovirus for expression in SF9 cells, as previously described (43).

ATPase Assays and Transient Kinetics. Actin-activated ATPase assays and transient kinetic measurements shown in Table 1 were performed as described (22, 43). Briefly, steady-state ATPase activities were measured at 25 °C in KMg50 buffer (50 mM KCl, 1 mM MgCl₂, 1 mM EGTA, 1 mM DTT, and 10 mM imidazole; pH 7.0 at 25 °C) to which 1 mM MgATP was added and then supplemented with the NADH-coupled assay components (44). Transient kinetic measurements were made in KMg50 buffer at 25 °C with an Applied Photophysics SX.18MV stopped-flow having a 1.2-ms dead time. A 400-nm colored glass emission filter was used to monitor pyrene (λ_{ex} = 365 nm), mantADP (λ_{ex} = 365 nm), mantATP (λ_{ex} = 365 nm), or NADH (λ_{ex} = 340 nm) fluorescence. Nonlinear least-squares fitting of the data was done with software provided with the instrument or with KaleidaGraph (Synergy Software). Uncertainties reported are SEs in the fits of three or four independent protein preparations and sets of measurements.

Crystallization, X-Ray Data Collection, and Structure Determination. The myosin VI D179Y MD^{ins2} mutant was crystallized in the rigor state (34) using the hanging drop vapor diffusion method at 4 °C by 1 μ L of 20 mg/mL protein solution mixed with 1 μ L of reservoir solution [4.5% (wt/vol) PEG 8000, 50 mM Mops (pH 7), 3% isopropanol, 3% *tert*-butanol, and 1 mM TCEP]. The crystals were cryoprotected in the reservoir solution complemented with 20% of ethylene glycol and flash-frozen in liquid nitrogen.

Crystals of myosin VI D179Y Δ -insert1 MD^{ins2} in the postrigor state were grown using reservoir solution [containing 10% PEG 8000, 50 mM Tris (pH 8.5), 1 mM TCEP, and 6% MPD] and stock solution of Δ -insert1 myosin VI at 17 mg/mL with MgADP BeFx bound (35). The protein/precipitant drops were microseeded the next day by streak-seeding from previous crystallizations and crystals appeared overnight. The crystals were cryoprotected in the reservoir solution complemented with 20% of MPD and flash-frozen in liquid nitrogen.

Crystals of myosin VI D179Y MD in the PPS state were grown using reservoir solution [containing 5.5% PEG 8000, 50 mM Tris (pH 8.5), 50 mM KSCN, 5% glycerol, and 20 mM DTT] and stock solution of myosin VI MD at 5 mg/mL with MgADP VO4 bound (33). The protein/precipitant drops were microseeded the next day by streak-seeding from previous crystallizations and crystals appeared overnight. The crystals were cryoprotected in the reservoir solution complemented with 20% of MPD and flash-frozen in liquid nitrogen.

X-ray diffraction data were collected at 100 K at the Soleil synchrotron radiation source, beamline Proxima 1, or the European Synchrotron Radiation Facility beamline ID-23-1. The data were processed using the XDS program suite (45, 46).

The mutant MVI crystal structures were determined by the molecular replacement method with MOLREP (47, 48) using the WT myosin VI structures corresponding to each conformational state [PDB ID codes 2BKX (rigor), 2VAS (postrigor), and 2V26 (PPS)] as search models. Several iterative cycles of crystallographic refinement with Refmac5 and PHENIX (47, 49) followed by manual model rebuilding with Coot (50) were performed to obtain the final structures deposited to the Protein Data Bank (4DBP for D179Y MD^{ins2} in the rigor state, 4DBQ for Δ -insert1 MD^{ins2} in the postrigor state, and 4DBR for MD in the PPS state). Table S1 lists the data collection and refinement statistics. All diagrams for the figures were computed using PyMOL (51).

Assays of In Vitro Gliding Motility and Single-Molecule Motility and Determination of Run Length and Velocity. The sliding actin filament assay was conducted at 30 °C similarly to the procedure described by Sweeney et al. (42). A FIONA type of assay (52) was used for single-molecule motility measurement. The procedure was essentially the same as described by Phichith et al. (40) except that the myosin constructs (wild or mutant) in the current study were constitutive dimers and were fluorescently labeled by exchange of a Cy3-conjugated CaM (at residue 146) onto the IQ-CaM, as previously described (53). For sliding motility assay, the assay was conducted in the buffer containing 50 mM KCl, 50 mM Imidazole (pH 7.4), 2 mM EGTA, 8 mM MgCl₂, 2 mM ATP, 5 μ M calmodulin, 20 mM DTT, 25 μ g/mL glucose oxidase, 45 μ g/mL catalase, 1% glucose, 1 mM creatine phosphate, and 0.1 mg/mL creatine phosphokinase, with or without 10 μ M ADP. The single-molecule motility was assayed in the buffer based on the KMg50 buffer as described above plus an oxygen scavenger system that contains 25 μ g/mL glucose oxidase and 45 μ g/mL catalase. High and low MgATP assay buffer conditions were then made by using BAD solution calculation program (54) to hold free Mg²⁺ concentration (1 mM) and ionic strength (65 mM) constant. The gliding and single-molecule motilities were imaged by using a Multi-Color Leica AM TIRF MC system equipped with integrated solid-state 405-nm, 488-nm, 561-nm, and 635-nm lasers along with GFP, VEG, Cy3, and Y35 filter cubes. A high-sensitivity and high-speed EMCCD camera (ImagEM-CCD Camera C9100-13; Hamamatsu Corporation) was used with the system for image acquisition. The run length and velocity were defined and determined as described

by Sweeney et al. (42). The acquiring frame rate of three frames per second was used. Individual trajectories were extracted and measured from image sequences in ImageJ (NIH) by using the MTrack2 plug-in developed in the Vale laboratory at University of California, San Francisco. Trajectories of minimum three frames (1 s) and 0.3- μ m minimum distance traveled were scored as processively moving motors. Although the run length and run time were automatically tracked with MTrack2, the quality of tracking was further verified by manual validation of each tracked trajectory. The run length is reported as arithmetic mean run length and the length decay constant λ . The mean run length was determined by averaging pooled data. The run length decay constant λ was analyzed by nonlinear least-squares fitting of cumulative distribution from $\times 0$ to infinity to

$1 - \exp[-(X0 - X/\lambda)]$ as described by Thorn et al. (55). GraphPad Prism 6 (GraphPad Software, Inc.) was used for statistical analysis, curve fitting, and data plotting.

ACKNOWLEDGMENTS. We thank Xiaoyan Liu and Alan B. Zong for their technical contributions. This work was done by a team (A.M.H.) belonging to the labex CelTisPhyBio 11-LBX-0038. O.P. is the recipient of an Association de la Recherche contre le Cancer (ARC) postdoctoral fellowship. This work was supported by a grant from NIH (DC009100) (to H.L.S.), CNRS (A.M.H.), the ARC subvention fixe (ARC 1067) 1067XA0830F, a Fondation pour la Recherche Médicale Equipe 2010 grant, and the Agence Nationale de la Recherche Blanche BLAN 2010 and 2014 (A.M.H.).

- Wells AL, et al. (1999) Myosin VI is an actin-based motor that moves backwards. *Nature* 401(6752):505–508.
- Rock RS, et al. (2001) Myosin VI is a processive motor with a large step size. *Proc Natl Acad Sci USA* 98(24):13655–13659.
- Nishikawa S, et al. (2002) Class VI myosin moves processively along actin filaments backward with large steps. *Biochem Biophys Res Commun* 290(1):311–317.
- Altman D, Sweeney HL, Spudich JA (2004) The mechanism of myosin VI translocation and its load-induced anchoring. *Cell* 116(5):737–749.
- Buss F, Spudich G, Kendrick-Jones J (2004) Myosin VI: Cellular functions and motor properties. *Annu Rev Cell Dev Biol* 20:649–676.
- Tumbarello DA, Kendrick-Jones J, Buss F (2013) Myosin VI and its cargo adaptors - linking endocytosis and autophagy. *J Cell Sci* 126(Pt 12):2561–2570.
- Sweeney HL, Houdusse A (2007) What can myosin VI do in cells? *Curr Opin Cell Biol* 19(1):57–66.
- Sweeney HL, Houdusse A (2010) Myosin VI rewrites the rules for myosin motors. *Cell* 141(4):573–582.
- Heintzelman MB, Hasson T, Mooseker MS (1994) Multiple unconventional myosin domains of the intestinal brush border cytoskeleton. *J Cell Sci* 107(Pt 12):3535–3543.
- Buss F, Arden SD, Lindsay M, Luzio JP, Kendrick-Jones J (2001) Myosin VI isoform localized to clathrin-coated vesicles with a role in clathrin-mediated endocytosis. *EMBO J* 20(14):3676–3684.
- Biemesderfer D, Mentone SA, Mooseker M, Hasson T (2002) Expression of myosin VI within the early endocytic pathway in adult and developing proximal tubules. *Am J Physiol Renal Physiol* 282(5):F785–F794.
- Morris SM, et al. (2002) Myosin VI binds to and localises with Dab2, potentially linking receptor-mediated endocytosis and the actin cytoskeleton. *Traffic* 3(5):331–341.
- Warner CL, et al. (2003) Loss of myosin VI reduces secretion and the size of the Golgi in fibroblasts from Snell's waltzer mice. *EMBO J* 22(3):569–579.
- Dance AL, et al. (2004) Regulation of myosin-VI targeting to endocytic compartments. *Traffic* 5(10):798–813.
- Vreugde S, et al. (2006) Nuclear myosin VI enhances RNA polymerase II-dependent transcription. *Mol Cell* 23(5):749–755.
- Melchionda S, et al. (2001) MYO6, the human homologue of the gene responsible for deafness in Snell's waltzer mice, is mutated in autosomal dominant nonsyndromic hearing loss. *Am J Hum Genet* 69(3):635–640.
- Ahmed ZM, et al. (2003) Mutations of MYO6 are associated with recessive deafness, DFNB37. *Am J Hum Genet* 72(5):1315–1322.
- Mohiddin SA, et al. (2004) Novel association of hypertrophic cardiomyopathy, sensorineural deafness, and a mutation in unconventional myosin VI (MYO6). *J Med Genet* 41(4):309–314.
- Avraham KB, et al. (1995) The mouse Snell's waltzer deafness gene encodes an unconventional myosin required for structural integrity of inner ear hair cells. *Nat Genet* 11(4):369–375.
- Hertzano R, et al. (2008) A Myo6 mutation destroys coordination between the myosin heads, revealing new functions of myosin VI in the stereocilia of mammalian inner ear hair cells. *PLoS Genet* 4(10):e1000207.
- Yildiz A, et al. (2004) Myosin VI steps via a hand-over-hand mechanism with its lever arm undergoing fluctuations when attached to actin. *J Biol Chem* 279(36):37223–37226.
- De La Cruz EM, Ostap EM, Sweeney HL (2001) Kinetic mechanism and regulation of myosin VI. *J Biol Chem* 276(34):32373–32381.
- Rosenfeld SS, Sweeney HL (2004) A model of myosin V processivity. *J Biol Chem* 279(38):40100–40111.
- Sweeney HL, et al. (2007) How myosin VI coordinates its heads during processive movement. *EMBO J* 26(11):2682–2692.
- Pylpenko O, et al. (2011) Role of insert-1 of myosin VI in modulating nucleotide affinity. *J Biol Chem* 286(13):11716–11723.
- Sahlender DA, et al. (2005) Optineurin links myosin VI to the Golgi complex and is involved in Golgi organization and exocytosis. *J Cell Biol* 169(2):285–295.
- Bond LM, Peden AA, Kendrick-Jones J, Sellers JR, Buss F (2011) Myosin VI and its binding partner optineurin are involved in secretory vesicle fusion at the plasma membrane. *Mol Biol Cell* 22(1):54–65.
- Seiler C, et al. (2004) Myosin VI is required for structural integrity of the apical surface of sensory hair cells in zebrafish. *Dev Biol* 272(2):328–338.
- Elting MW, Bryant Z, Liao J-C, Spudich JA (2011) Detailed tuning of structure and intramolecular communication are dispensable for processive motion of myosin VI. *Biophys J* 100(2):430–439.
- Coureux P-D, Sweeney HL, Houdusse A (2004) Three myosin V structures delineate essential features of chemo-mechanical transduction. *EMBO J* 23(23):4527–4537.
- Coureux P-D, et al. (2003) A structural state of the myosin V motor without bound nucleotide. *Nature* 425(6956):419–423.
- Bahloul A, et al. (2004) The unique insert in myosin VI is a structural calcium-calmodulin binding site. *Proc Natl Acad Sci USA* 101(14):4787–4792.
- Ménétrey J, Llinas P, Mukherjee M, Sweeney HL, Houdusse A (2007) The structural basis for the large powerstroke of myosin VI. *Cell* 131(2):300–308.
- Ménétrey J, et al. (2005) The structure of the myosin VI motor reveals the mechanism of directionality reversal. *Nature* 435(7043):779–785.
- Ménétrey J, et al. (2008) The post-rigor structure of myosin VI and implications for the recovery stroke. *EMBO J* 27(1):244–252.
- Malik FI, et al. (2011) Cardiac myosin activation: A potential therapeutic approach for systolic heart failure. *Science* 331(6023):1439–1443.
- Sun M, et al. (2006) Dynamics of the upper 50-kDa domain of myosin V examined with fluorescence resonance energy transfer. *J Biol Chem* 281(9):5711–5717.
- Sato O, et al. (2004) Human deafness mutation of myosin VI (C442Y) accelerates the ADP dissociation rate. *J Biol Chem* 279(28):28844–28854.
- Mukherjee M, et al. (2014) Myosin VI must dimerize and deploy its unusual lever arm in order to perform its cellular roles. *Cell Reports* 8(5):1522–1532.
- Pichith D, et al. (2009) Cargo binding induces dimerization of myosin VI. *Proc Natl Acad Sci USA* 106(41):17320–17324.
- Lumb KJ, Carr CM, Kim PS (1994) Subdomain folding of the coiled coil leucine zipper from the bZIP transcriptional activator GCN4. *Biochemistry* 33(23):7361–7367.
- Sweeney HL, et al. (1998) Kinetic tuning of myosin via a flexible loop adjacent to the nucleotide binding pocket. *J Biol Chem* 273(11):6262–6270.
- De La Cruz EM, Wells AL, Rosenfeld SS, Ostap EM, Sweeney HL (1999) The kinetic mechanism of myosin V. *Proc Natl Acad Sci USA* 96(24):13726–13731.
- De La Cruz EM, Sweeney HL, Ostap EM (2000) ADP inhibition of myosin V ATPase activity. *Biophys J* 79(3):1524–1529.
- Kabsch W (2010) XDS. *Acta Crystallogr D Biol Crystallogr* 66(Pt 2):125–132.
- Diederichs K, McSweeney S, Ravelli RBG (2003) Zero-dose extrapolation as part of macromolecular synchrotron data reduction. *Acta Crystallogr D Biol Crystallogr* 59(Pt 5):903–909.
- Vagin A, Teplyakov A (1997) MOLREP: An automated program for molecular replacement. *J Appl Cryst* 30:1022–1025.
- Collaborative Computational Project, Number 4 (1994) The CCP4 suite: Programs for protein crystallography. *Acta Crystallogr D Biol Crystallogr* 50(Pt 5):760–763.
- Adams PD, et al. (2010) PHENIX: A comprehensive Python-based system for macromolecular structure solution. *Acta Crystallogr D Biol Crystallogr* 66(Pt 2):213–221.
- Emsley P, Cowtan K (2004) Coot: Model-building tools for molecular graphics. *Acta Crystallogr D Biol Crystallogr* 60(Pt 12 Pt 1):2126–2132.
- DeLano WL (2002) PyMOL molecular graphics system, Version 1.7.4. Available at www.pymol.org. Accessed February 18, 2015.
- Yildiz A, Selvin PR (2005) Fluorescence imaging with one nanometer accuracy: Application to molecular motors. *Acc Chem Res* 38(7):574–582.
- Park H, et al. (2006) Full-length myosin VI dimerizes and moves processively along actin filaments upon monomer clustering. *Mol Cell* 21(3):331–336.
- Brooks SPJ, Storey KB (1992) Bound and determined: A computer program for making buffers of defined ion concentrations. *Anal Biochem* 201(1):119–126.
- Thorn KS, Ubersax JA, Vale RD (2000) Engineering the processive run length of the kinesin motor. *J Cell Biol* 151(5):1093–1100.